High-Density Electromyography and Motor Skill Learning for Robust Long-Term Control of a 7-DoF Robot Arm

Mark Ison, Ivan Vujaklija, Bryan Whitsell, Dario Farina and Panagiotis Artemiadis

***Abstract*—Myoelectric control offers a direct interface between human intent and various robotic applications through recorded muscle activity. Traditional control schemes realize this interface through direct mapping or pattern recognition techniques. The former approach provides reliable control at the expense of functionality, while the latter increases functionality at the expense of long-term reliability. An alternative approach was recently proposed using concepts of motor learning. It provides session-independent simultaneous control, but previously relied on consistent electrode placement over biomechanically independent muscles. This paper extends the functionality and practicality of the motor learning-based approach, using high-density electrode grids and muscle synergy-inspired decomposition to generate control inputs with reduced constraints on electrode placement. The method is demonstrated via real-time simultaneous and proportional control of 4-DoF while operating a myoelectric interface over multiple days. Subjects showed learning trends consistent with typical motor skill learning without requiring any retraining or recalibration between sessions. Moreover, they adjusted to physical constraints of a robot arm after learning the control in a constraint-free virtual interface, demonstrating robust control as they performed precision tasks. The results demonstrate the efficacy of the proposed man-machine interface as a viable alternative to conventional control schemes for myoelectric interfaces designed for long-term use.**

***Index Terms*—Electromyography, Human-Robot Interaction, Motor Learning, Myoelectric Control, Simultaneous Control, High-Density EMG, Real-Time Systems, Prosthetics**

I. Introduction

Myoelectric control allows a convenient human-machine interface by transforming electromyography (EMG) signals into control outputs. Surface EMG (sEMG) provides non-invasive access to muscle activity. This type of control has been explored extensively due to its direct application to functional prostheses [1]–[3]. Recent extensions consider applications in other human-machine interfaces, such as robot teleoperation [4]–[6], powered wheelchairs [7] and virtual joysticks [8]. However, transient changes in sEMG cause a trade-off between functionality (i.e. proportional and simultaneous control) [9], [10] and reliability (i.e. consistent long-term control without frequent retraining) [11], [12] in most control schemes.

This study was financially supported by the European Research Council (ERC) via the ERC Advanced Grant DEMOVE (No. 267888). All authors declare no conflict of interests.

M. Ison, B. Whitsell, and P. Artemiadis are with the School for Engineering of Matter, Transport and Energy, Arizona State University, Tempe, AZ 85287-6106 USA (e-mail: panagiotis.artemiadis@asu.edu).

I. Vujaklija and D. Farina are with the Department of Neurorehabiliation Engineering, Bernstein Focus Neurotechnology Göttingen, Bernstein Center for Computational Neuroscience, University Medical Center Göttingen, Georg-August University, 37075 Göttingen, Germany (e-mail: dario.farina@bccn.uni-goettingen.de).

Two control approaches are currently employed in conventional myoelectric control: direct control and pattern recognition (PR). Direct control links antagonistic muscles or muscle groups directly to a single degree-of-freedom (DoF) [13]. Various switching methods sequentially transition between different DoFs or functions in finite state machines [14]. These simplistic controllers provide reliable controls, but lack the functionality to smoothly operate multiple DoFs [15].

PR methods utilize machine learning techniques, including both classification [16] and regression [17], to decode a mapping between myoelectric inputs and desired outputs [1]. This enhances functionality compared to direct controls by enabling multiple DoFs without explicit switching methods. However, increased functionality requires an updated training set which is highly dependent on the user's motion repeatability [16] and influenced by many external factors [18]–[21]. Thus, the decoding often overfits to a small set of the full input space, and performance tends to degrade over time [22]. Adaptive [22]–[25] and pre-trained models [26]–[29] attempt to avoid this effect with varied success.

An alternative method was recently proposed utilizing concepts of motor skill learning and brain plasticity [30]. These motor learning-based methods extend direct control principles to multiple DoFs through linear transformations between EMG inputs and control outputs, naturally providing both simultaneous and proportional control [31]. The surjective mapping creates a redundancy in the control scheme which reduces the precision needed in muscle activations to control the entire task-space [32]. These methods have shown a user's ability to learn a given mapping, regardless of its intuitiveness [33], and to develop muscle synergies associated with enhanced control of the myoelectric interface [34], [35].

While these motor learning implementations consistently demonstrate session-independence, they rely on targeted electrode placement over biomechanically independent muscles to avoid biomechanical constraints [36] and to enhance learning potential [33], [35]. Robust extensions to three or more DoFs originally required a large number of input muscles [37] to maintain redundancy in the control scheme and to avoid unintended outputs during use [32]. However, Ison and Artemiadis [38] introduced a surjective mapping function enabling robust simultaneous control of 3-DoFs using only four independent muscle inputs.

This work presents a novel myoelectric control scheme capable of real-time simultaneous and proportional control of a large number of DoFs, without requiring retraining between sessions, targeted electrode placement, nor biomechanically independent muscle inputs. A novel muscle synergy-inspired decomposition transforms high-density (HD) sEMG into independent activation signals which linearly map to control outputs. The algorithm (detailed in Section III-A2) extends the DoF-wise non-negative matrix factorization (NMF) algorithm proposed by Jiang et al. [39]. DoF-wise NMF extracts muscle synergies related to hand kinematics, and the extension transforms these synergies into independent activation signals to ensure the outputs can be operated autonomously for complete simultaneous and proportional control of the interface. The method is demonstrated using concurrent control of 4-DoFs in a finite state machine (FSM) to control a 7-DoF robot arm, and validated via learning trends and session-independent characteristics identified in other motor learning-based schemes [30]–[35], [38]. To the best of the authors' knowledge, no other myoelectric control scheme has demonstrated real-time simultaneous and proportional control of 4-DoFs from untargeted sEMG of a single arm. Moreover, previous attempts at myoelectric control of a 7-DoF robot arm required retraining each session [40], [41].

II. Related Work

A. Motor Learning

Learning a new motor task typically involves a three stage learning process [42]. The initial cognitive stage carries a significant mental load and sporadic performance as users explore and gather information relevant to the task. As users repeat the task, they enter an associative stage with reduced conscious effort and increased performance. Finally, through repetition, an autonomous stage is reached, where tasks seem unconscious and intuitive to perform [42].

These principles are associated with brain plasticity and commonly utilized in brain-machine interfaces [43], which train users to associate thoughts with controls [44]. Similar learning trends are seen with myoelectric interfaces. Users adapt to controls within a single session regardless of their initial intuitiveness or relationship with kinematics [30], [32], [33], [45]. Radhakrishnan et. al [30] found that this initial adaptation results in an exponential performance enhancement. Antuvan et. al [33] observed that less intuitive controls have worse initial performance, but a higher learning rate such that performance quickly converges with that obtained using more intuitive control schemes. These adaptations are associated with the dynamic formation of new muscle synergies, resulting in more efficient control of the interface as users presumably enter the later stages of motor learning [34], [35]. Ison and Artemiadis found a correlation between these developing muscle synergies and a long term learning component, both of which contribute to performance retention among similar tasks, efficient generalization to new tasks, and effective transfer to new interfaces [31], [34].

Clingman et. al [46] propose that these characteristics can be applied to entertaining myoelectric training systems for more robust interaction with prosthetic devices. Ison and Artemiadis [38] demonstrated the potential benefits of such a training system as subjects implicitly learned to control a robot arm by interfacing with an analogous virtual object via a non-intuitive control scheme. The subjects naturally transferred this learning when interacting with the physical robot, feeling the controls were intuitive despite them having no relation to human kinematics.

All of the above control schemes target specific, biomechanically independent muscles for interaction with the interface. De Rugy et. al [36] noted that dependent muscles may hinder motor learning and prevent users from obtaining satisfactory performance while interacting with abstract myoelectric interfaces. The present work incorporates high density surface electromyography to eliminate this constraint and expand the capabilities of motor learning in myoelectric interfaces.

B. High-Density sEMG

sEMG signals are influenced by a variety of factors and transient changes which can render individual signals unreliable [1], [47], [48]. While many of these complications can be eliminated with invasive measures [49], they can be significantly reduced by recording a richer information set from HD electrodes without requiring exact electrode placement.

Untargeted electrodes uniformly placed around the forearm has become standard for PR-based myoelectric controls in recent years [15], [50], [51]. HD extensions use electrode grids to extract 2D information from the muscle activity [52]. Muceli et. al [53] used these grids in a simultaneous 4-DoF control scheme trained with multi-layer perceptrons, but only evaluated results offline. Tkach et. al [54] used similar grids to train a linear discriminant analysis classifier on arm and hand motions for subjects with amputations, concluding that the richer processing led to more robust control. Unfortunately, the increased number of signals bring enhanced concerns for overfitting, limiting such PR controls during long-term use.

Alternative control techniques with HD sEMG propose semi-unsupervised methods. Jiang et. al [39] introduced a muscle synergy-inspired extraction method for motions along desired DoFs in the control scheme. Multiplying input signals with the obtained weights provides simultaneous control for an intuitive motor learning-like 2-DoF control scheme [55], [56]. Muceli et. al [57] demonstrated how these controls may be robust to different electrode number, shifts, and configurations. Although promising, these controls have yet to demonstrate session-independence for operation of more than 2-DoFs. This work adapts these methods to generate a session-independent control scheme capable of controlling more DoFs.

III. Methods

The experiment performed in this study evaluates performance characteristics and control capabilities of a novel control scheme operating a 7-DoF myoelectric interface with 4-DoF simultaneous and proportional control. Three sessions are conducted on distinct days. In the first two sessions, a user learns the control scheme by interacting with a helicopter in virtual reality (VR) to complete a set of tasks. The final session involves controlling a KUKA Light Weight Robot 4 (LWR 4) and an attached Touch Bionics iLIMB Ultra to complete three precision tasks using the same control scheme. Subjects are split into two groups. The experimental group interacts with the two interfaces via HD sEMG inputs, while the control group uses keyboard inputs. The control group acts as a reference for learning using definitive, noiseless inputs on the non-intuitive control scheme.

A. Muscle Synergy-Inspired Decomposition

Muscle synergy-inspired dimensionality reduction extracts robust control information from HD sEMG by separating redundant signals into quasi-independent inputs.

1) Muscle Synergy Based Model: Jiang et. al [39] modeled HD sEMG observations, $\mathbf{Y}(t)$, as instantaneous mixtures of muscle activation signals, $\mathbf{F}(t)$. Following the notation in Muceli et. al [57], the relationship is defined as:

$$\mathbf{Y}(t) = \mathbf{W} \cdot \mathbf{F}(t) \tag{1}$$

where $\mathbf{W}$ is a channel weighting matrix representing the contribution of the activation signals to the signal received at each electrode. Each column $\mathbf{W}_i$ approximates a muscle synergy provided as high-level input by a user when interacting with myoelctric interfaces [1]. This model is proposed as the basis for extracting robust control signals from HD sEMG [57], and is similarly used as the basis for this control paradigm.

$\mathbf{W}$ is generated using the DoF-wise NMF algorithm described in [39]. This algorithm assumes that two activation signals control a single DoF on a joint, one in the positive direction, $f_i^+(t)$, and one in the negative, $f_i^-(t)$. Thus, $\mathbf{W}$ becomes a $n \times m$ matrix, where $m = 2d$, with n sEMG channels and d DoFs of interest [39]:

$$\mathbf{Y}(t) = [\mathbf{W}_1^+\mathbf{W}_1^- \cdots \mathbf{W}_d^+\mathbf{W}_d^-] \cdot \begin{bmatrix} f_1^+(t) \\ f_1^-(t) \\ \vdots \\ f_d^+(t) \\ f_d^-(t) \end{bmatrix} \tag{2}$$

2) Novel Activation Signal Extraction: This paper proposes a novel method to extract $k < m$ quasi-independent activation signals by approximating a subset of k independent columns in $\mathbf{W}$. If all $\mathbf{W}_i$ are orthonormal, $\mathbf{W}$ is a semi-orthogonal matrix satisfying $\mathbf{W}^T\mathbf{W} = I$, and the left inverse of $\mathbf{W}$ exists: $\mathbf{W}_{left}^{-1} = \mathbf{W}^T$. $\mathbf{Y}(t)$ can then be decomposed into independent activation signals:

$$\mathbf{F}(t) = \mathbf{W}^T \cdot \mathbf{Y}(t), \tag{3}$$

providing independent control inputs to the interface.

The DoF-wise NMF algorithm does not guarantee a semi-orthogonal $\mathbf{W}$. Moreover, the variability of sEMG causes uncertainty in the exact values of $\mathbf{W}$. The proposed algorithm produces a $n \times k$ semi-orthogonal matrix, $\hat{\mathbf{W}}$, decomposing sEMG into quasi-independent control inputs, $\hat{\mathbf{F}}(t)$, approximating activation signals $\mathbf{F}(t)$. Given the 4×4 Gaussian kernel $\mathbf{G}$, function $\delta(\mathbf{V})$ thresholding $\mathbf{V}$ to 0 at one standard deviation below the maximum element in $\mathbf{V}$, and 2D convolution operator $*$, the algorithm generating $\hat{\mathbf{W}}$ is as follows:

1) Rearrange all $\mathbf{W}_i$ according to the 2D configuration of the HD electrode grid.
2) $\forall \mathbf{W}_i \ (i \in \{1..m\}) : \mathbf{W}'_i = \delta(\mathbf{W}_i) * \mathbf{G}$.
3) $m - k$ times do: Merge $\mathbf{W}'_a$ and $\mathbf{W}'_b$, where $\mathbf{W}'_a$ and $\mathbf{W}'_b$ have the closest cosine similarity of all $\mathbf{W}'_i$ pairs.
4) $\forall \mathbf{W}'_i \ (i \in \{1..k\}) : \mathbf{W}'_i = \delta(\mathbf{W}'_i) * \mathbf{G}$.
5) $\forall \mathbf{W}'_i : \hat{\mathbf{W}}_i = \frac{\mathbf{W}'_i}{|\mathbf{W}'_i|}$, reshaped to a row vector.

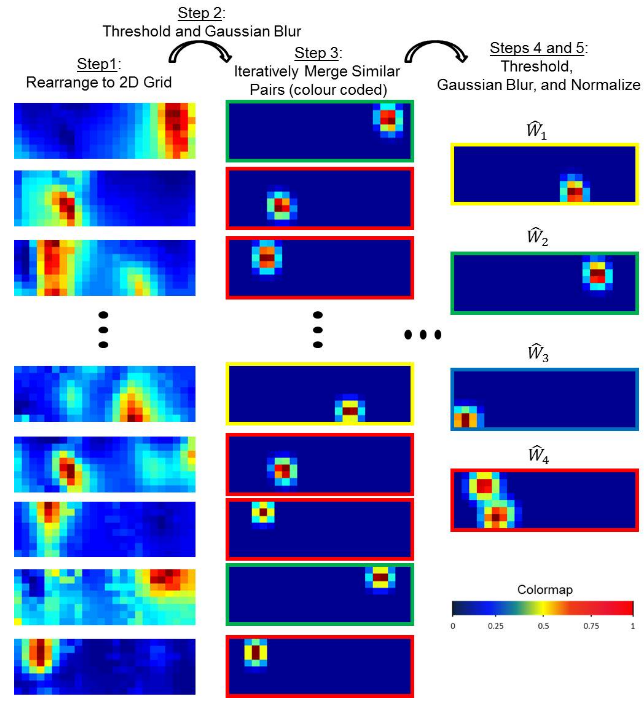

Fig. 1. Summary of the proposed 5-step algorithm to generate $\hat{\mathbf{W}}$ with four quasi-independent control inputs from a noisy $\mathbf{W}$. Each column of both $\mathbf{W}$ and $\hat{\mathbf{W}}$ is represented with elements rearranged according to their topographic position on high-density electrode grids, as described in Fig. 3 below.

Figure 1 demonstrates the algorithm visually. $\hat{\mathbf{W}}$, with Gaussian blurred, orthonormal columns, satisfies (3) and forms the basis of a session-independent control scheme. The mixture of Gaussians, represented by $\hat{\mathbf{W}}$, act as a spatial low-pass filter on the noisy EMG input signals. The sparser $\hat{\mathbf{W}}$ also reduces the influence of cross-talk for easier isolation of control outputs and enhanced simultaneous control. The consistency of the resulting decomposition is a function of overlap between the approximated activation signals and the user's true underlying activation points. By only considering independent activation points, the robustness is a function of electrode span within and electrode distance between each activation signal versus potential electrode displacement.

B. Experimental Setup

The VR and robot control setups for the experimental group are shown in Fig. 2 and 2(b), respectively. HD sEMG signals are recorded from the right forearm muscles, approximately two inches below the elbow at the ulnar bone, using three equally spaced semi-disposable adhesive 8×8 electrode grids, with 10mm inter-electrode distance. In contrast to previous studies involving multiple sessions with untargeted electrodes [22], exact electrode positioning was not marked in this study to simulate cross-session performance in a realistic use scenario. The skin is cleansed with water and a reference electrode is placed on the subject's elbow.

The 192 monopolar signals are acquired using EMG-USB2, OT Bioelettronica amplifier with gain set to 1000, bandpass filtered at $3 - 900Hz$, sampled at $2048Hz$ with 12-bit A/D

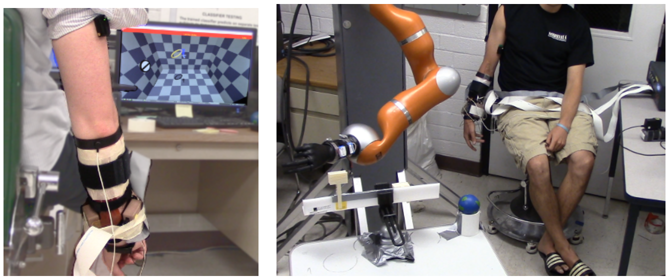

(a) (b)

Fig. 2. Experimental setup with HD sEMG electrodes. (a) Session 1 and 2: VR interface controlling a helicopter's position, orientation, and color. (b) Session 3: LWR 4, iLIMB, and three target objects to grasp and move based on controls learned in the VR interface.

TABLE I
FINITE STATE MACHINE CONTROL AXES

Control Axis	Position State	Orientation State
1	X	Yaw (ϕ)
2	Y	Pitch (θ)
3	Z	Roll (ρ)
4	Color (VR) or Hand Open/Close (Robot)	

conversion, and broadcast via TCP for further processing, as in [57]. Two additional sEMG signals are recorded on the biceps brachii (BB) and triceps brachii (TB) using wireless electrodes (Delsys Trigno Wireless, Delsys Inc.). These bipolar electrodes are acquired with a gain of 500, digitized with 16-bit depth at a frequency of 1926 Hz and broadcast via TCP. Both signals are received by a custom program using C++ and OpenGL API [58] to control both interfaces. The sEMG signals are processed in real-time and converted to control variables of the virtual helicopter (session 1 and 2) or robotic hand (session 3). The helicopter and hand respond to the outputs at $200Hz$.

C. Control Paradigm

The 7-DoF control scheme is implemented as a two-state finite state machine, with each state offering simultaneous control of velocities over 4-DoFs (see Table I). Control Axes 1-3 switch between controlling the global position and local orientation of the object. Co-contracting both BB and TB above a preset threshold induces the switch. Control Axis 4 is constant among both states, controlling the color of the helicopter and hand opening/closing of the robot.

The input sEMG is pre-processed to provide linear envelopes as input, $\mathbf{Y}(t)$. The mapping function is adapted from [34], with a linear mapping between the 194×1 vector $\mathbf{Y}(t)$ $(3 * 64 + 2)$ and 4×1 vector $\mathbf{U}(t)$ of control outputs:

$$\mathbf{U}(t) = g\mathbf{M} \cdot \hat{\mathbf{W}}^{\mathbf{T}} \cdot \left[(\mathbf{Y}(t) - \sigma) \circ u(\mathbf{Y}(t) - \sigma)\right], \quad (4)$$

where $\circ$ is an element-wise matrix multiplication, $u(*)$ is the unit step function, σ is the muscle activation threshold, and g is the output gain. $\hat{\mathbf{W}}$ is the muscle synergy-inspired 194×6 decomposition matrix reducing $\mathbf{Y}(t)$ to quasi-independent control inputs $\hat{\mathbf{F}}(t)$, as described previously. $\mathbf{M}$ is a semi-random mixing matrix converting $\hat{\mathbf{F}}(\mathbf{t})$ to the control outputs $\mathbf{U}(t)$. The resultant $\mathbf{U}(t)$ is averaged over the last five outputs to reduce effects of any motion artifacts, electrode disconnections, or unintended muscle twitches. Both σ and g can be tuned for each subject, but in general, $\sigma = 0.01mV$ prevents undesired outputs from resting muscles and $g = 50$ provides a conservative sensitivity trade-off between too much and too little muscle activation required for movement.

1) Pre-Processing: Both sets of sEMG inputs are pre-processed to provide linear envelopes to the control scheme. The HD sEMG signals are first subtracted from the mean of all signals to remove external common noise, and then rectified and low-pass filtered (fourth-order zero-lag Butterworth filter, cut-off frequency $3Hz$). Finally, the signals are filtered by a 3×3 median filter to minimize the effects of any local disturbances. The additional TB and BB signals are rectified, low-pass filtered (fourth-order zero-lag Butterworth filter, cut-off frequency $3Hz$), and normalized with respect to the subject's maximal voluntary contraction (MVC), as found during the initial calibration. Both sets are sub-sampled to $200Hz$ and merged to $\mathbf{Y}(t)$, with TB and BB as the last elements.

2) Calibration: An initial calibration phase generates the session-independent $\hat{\mathbf{W}}$ unique for every subject, as described in Section III-A. With 192 HD electrodes spanning the circumference of the forearm, eight DoFs are considered here – four coarse wrist motions (wrist flexion/extension, wrist pronation/supination, ulnar/radial deviation, hand open/close) and four fine finger motions (flexion/extension of the index, middle, ring, and pinkie fingers). The calibration data was collected following the procedure described in [52]. Subjects were prompted by a monitor to move along each direction at a pace of roughly three seconds per motion. Each movement was repeated four times, summing to a total of 64 three-second recordings across the sixteen listed motions (half-DoFs) used to initialize a 192×16 $\mathbf{W}$.

Because the TB and BB are not part of the HD grid, their contribution is ignored until after the initial calculation of $\hat{\mathbf{W}}$ with $k = 4$. The contribution of both TB and BB are then appended to the fifth and sixth columns of $\hat{\mathbf{W}}$ at the 193^{rd} and 194^{th} row, respectively, with the remaining elements in those rows and columns set to zero. Thus, the 194×6 $\hat{\mathbf{W}}$ has the first four control inputs decomposed from forearm muscles (see Fig. 3), and the final two coming from TB and BB.

During this calibration, subjects also performed their MVC for TB and BB to set the switching threshold at 50% of it.

3) Mixing Matrix: To generate a control scheme capable of spanning the entire task space with minimal inputs, the mixing matrix, $\mathbf{M}$, is a random matrix optimized with a cost function maximizing the angles between row vectors and subject to the following constraints, where $\mathbf{M}_i$ is a column vector in $\mathbf{M}$:

1) $\mathbf{M}_5 = [0, 0, 0, 1]^T$ and $\mathbf{M}_6 = -\mathbf{M}_5$ to disconnect grasping from motion.
2) $\forall \mathbf{M}_i : |\mathbf{M}_i| = 1$ for equal contribution from all inputs.
3) All row vectors are zero mean to prevent motion at rest.

For this experiment, $\mathbf{M}$ is as follows (see Fig. 4):

$$\mathbf{M} = \begin{bmatrix} 0.52 & -0.94 & 0.42 & 0.00 & 0.00 & 0.00 \\ 0.79 & 0.06 & -0.85 & 0.00 & 0.00 & 0.00 \\ -0.33 & -0.34 & -0.33 & 1.00 & 0.00 & 0.00 \\ 0.00 & 0.00 & 0.00 & 0.00 & 1.00 & -1.00 \end{bmatrix} \quad (5)$$

4) Robot Control: The robot control runs slightly different than the controls within VR due to joint limits, singularities,

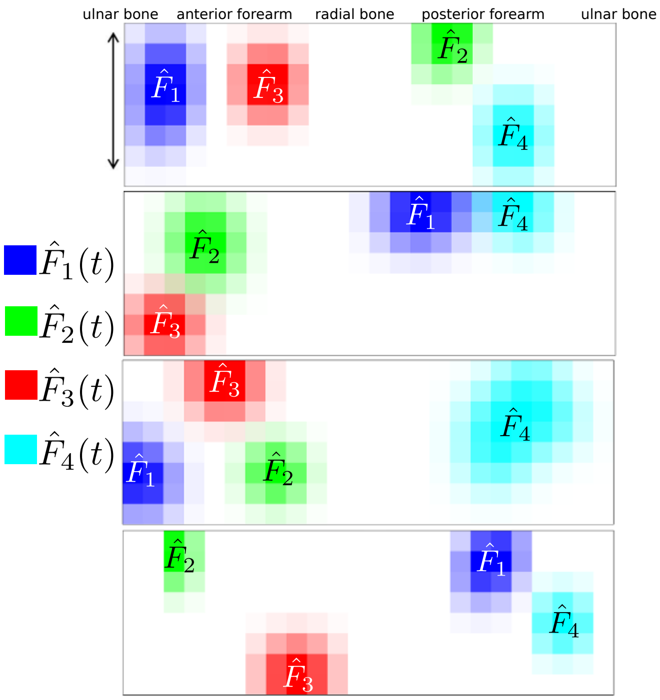

Fig. 3. Visualization of the first four columns of the muscle-synergy inspired decomposition matrix $\hat{\mathbf{W}}$, transforming high density sEMG $\mathbf{Y}(t)$ to four of the six quasi-independent control inputs $\hat{\mathbf{F}}(\mathbf{t})$. Each column $\hat{\mathbf{W}}_i$ is represented by a color, with elements rearranged according to their topographic position on the HD electrode grids. The intensity of the color indicates the weight of the elements in $\hat{\mathbf{W}}_i$. prox: proximal, dist: distal. This representation shows the three 8×8 grids as if they were contiguous around the circumference of the arm. In reality, each grid is separated by some distance depending on the subject's forearm circumference.

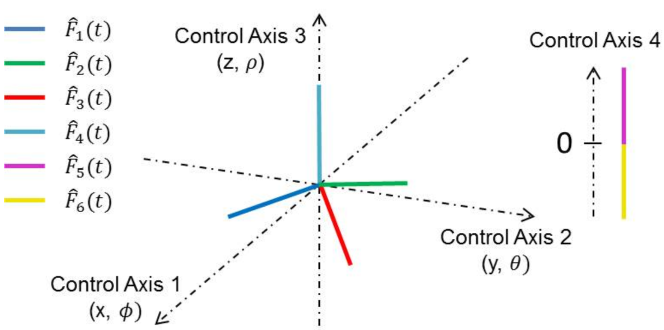

Fig. 4. Visualization of mapping $\mathbf{M}$, transforming control inputs $\hat{\mathbf{F}}(t)$ to four output control axes $\mathbf{U}(t)$, where each axis is as defined in Table I.

and torques. LWR 4 operates in Cartesian impedance control using inverse kinematics when the control state is in position, and joint impedance control using forward kinematics of the wrist joints when the control state is in orientation mode. The switch to joint impedance reduces the risk of exceeding joint velocity and position limits while rotating through singularities in the null space. Global ρ, ϕ, and θ are limited to $\pm\frac{\pi}{3}$ to avoid physical joint limitations while rotating. The iLIMB is controlled via velocity commands to all fingers over Bluetooth.

5) Noiseless Keyboard Interface: The control group uses keyboard inputs, with US layout, as $\hat{\mathbf{F}}(t)$, with simultaneous control offered by pressing multiple keys:

$$\mathbf{U}(t) = g\mathbf{M} \cdot \hat{\mathbf{F}}, \tag{6}$$

where $\mathbf{U}$, g, and $\mathbf{M}$ are defined as in (4), and visualized in Fig. 4. Subjects control color changes/hand grasping with their left hand ($\hat{F}_{5,6} = \{1, 2\}$) and position/orientation with their right hand ($\hat{F}_{1,2,3,4} = \{j, k, l, ;\}$) without needing to move their fingers off the keys. The magnitude of $\hat{F}$ was given by 90% of the maximum synergy input used by all subjects in the experimental group, allowing them to simulate proportional control by tapping the keys. This provides an ideal scenario for learning as subjects interact with the non-intuitive controls.

D. Experimental Protocol

Subjects interact with the control scheme over three sessions on distinct days. None of the subjects were initially aware how to control the interface, although they were shown how to switch between control states. They were asked to learn the simultaneous controls simply by interacting with them. The experimental group used sEMG inputs as described above, with an initial calibration phase before the first session to generate $\hat{\mathbf{W}}$ associated with the subject's underlying muscle anatomy. The control group used keyboard inputs as a noiseless substitute for sEMG.

1) Session 1: This session introduced the VR and its controls to the subject. All subjects were initially given 20 minutes to become familiar with the controls, in which example tasks were presented without requiring completion. Subjects were encouraged to explore the interface and understand how to control the helicopter along all 7 available DoFs. This time presumably encompasses the initial exponential learning documented previously [30], [32], [33].

After 20 minutes, subjects were asked to complete 26 tasks. At this point, it is expected that they will show more linear learning trends [34]. Each task consisted of three subtasks exercising control across all DoFs (see Fig. 5):

1) Move the helicopter to a ring displayed on the screen.
2) Rotate the helicopter toward a target displayed on a wall.
3) Change the helicopter's color to match the top bar cue.

Once the subject completed the full task, the helicopter returned to an initial position, orientation and color, and a ten second break was given. There was no task time limit to encourage exploration and reduce any effect of einstellung (i.e. becoming stuck in a non-optimal solution) while learning [59].

In total, subjects were presented 26 distinct rings uniformly placed on a sphere surrounding the starting point of the helicopter. 26 distinct orientation targets were also presented, uniformly spread on the walls along the front half of the VR space. Each trial presented a random combination of ring position, target position, and prompted color such that after 26 trials each ring and target position, respectively, were displayed exactly once. Thus, completing the full set on the first session ensures that the subject can move in the full task space. The random arrangement of ring, targets, and colors were constant for each subject to ensure a consistent learning environment.

2) Session 2: This session occured at least 24 hours after session 1. Subjects were asked to complete as many VR tasks as possible for one hour to evaluate learning retention. Subjects were not given any exploration time nor assistance during the

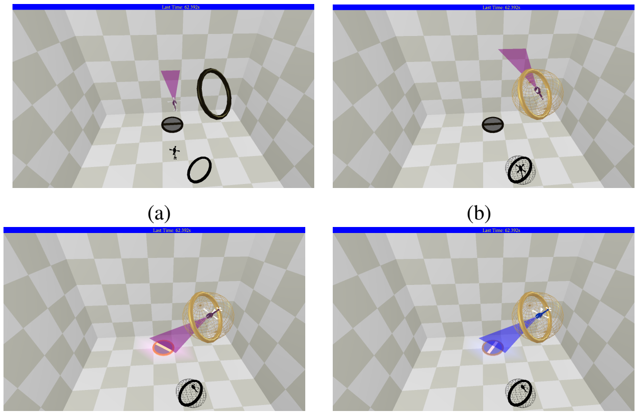

(a) (b) (c) (d)

Fig. 5. Subtask sequence for VR. The helicopter (a) starts from an initial configuration, (b) moves to the center of the ring, (c) rotates to point toward the target on the wall, (d) changes to the color shown in the top bar cue. The color task can be completed simultaneously, but (b) and (c) must be completed in order. Once all three subtasks are complete, the helicopter resets, and new ring, target, and color are shown after a 10 second rest.

(a) Clothespin 1 (b) Clothespin 2 (c) Ball

Fig. 6. Subtask sequence for the robot interface. The robot hand is controlled to grasp two clothespins (a and b, subject perspective) and a ball (c, top view). The object is then placed into the bin below the table. The order in which these tasks are completed is determined by each subject.

interaction, and use the same control scheme and $\hat{\mathbf{W}}$ calculated during session 1. Each cycle of 26 tasks presented a random combination of the complete sets of rings, targets, and colors from Session 1, held constant across subjects.

3) Session 3: The final session occured between one and eight days after session 2, and introduced the robot interface while still using the same control scheme and $\hat{\mathbf{W}}$ calculated during session 1. Subjects were asked to complete three precision tasks by sequentially grasping a tennis-sized ball and two customized clothespins to place in a bin. The clothespins were 3D printed extensions of conventional ones to provide a larger gripping area. The 2×1.25 inch grasping pad allowed two iLIMB digits to close on the area for a more stable grasp

Figure 2(b) shows the setup of the objects, with ideal grasps shown in Fig. 6. Subjects were required to activate all 7 DoFs with centimeter precision to grasp each object. The experiment was complete after grasping each object in any order.

E. Data Analysis

The first two sessions are split into eight equal blocks containing data from 25% of a single session, and performance metrics are compared among the control and experimental groups to determine the presence of motor learning. The final session records total completion time to indicate precision performance capabilities and any influential factors.

1) Learning Trends: During the first two sessions, performance is evaluated according to three metrics: completion time, throughput and path efficiency [60], [61]. Completion time, CT, is the time taken to successfully complete the task. Throughput, TP, measures both speed and accuracy by considering CT with respect to task difficulty, measured in bits/second according to Fitts' law standards [62]. Path efficiency, PE, is the ratio between the optimal distance, D, to complete the task and the actual path taken to reach the target [60]. . The index of difficulty, ID, of a task is given by the Shannon Formulation [62]:

$$ID = \log_2(\frac{D}{W_D} + 1) \tag{7}$$

where D is the optimal distance to complete the task and W_D is the weighted cumulative error tolerance of all targets, held constant throughout this experiment. D is formulated similar to [45]:

$$D = \frac{1}{g}\sqrt{(\lambda\gamma_1 + \gamma_2)^2 + \gamma_3^2} \tag{8}$$

where g is as defined in (4), γ_1 is the straight line distance from the starting position to the center of the ring, γ_2 is the angular distance between the starting orientation of the helicopter and the target orientation with respect to the center of the ring, γ_3 is the internal distance from starting color to desired color, and $\lambda = 0.471$ is the ratio between output angular velocity in orientation state and output velocity in position state for equal input $\hat{\mathbf{F}}(t)$. $gamma_1$ and $gamma_2$ are additive because the position and orientation subtasks are sequential, while color can be performed simultaneously. TP is then:

$$TP = \frac{ID}{CT} \tag{9}$$

The three metrics CT, TP and PE are evaluated with respect to block number b to form a mean model of the learning curve. Based on [34], the initial 20 minute exploration time presumably encapsulates the initial exponential learning component. Thus, the metrics are assumed to contain approximately linear trends, and are fit to first degree polynomials:

$$CT(b) = \kappa_{ct} - \beta_{ct} b \tag{10}$$

$$TP(b) = \kappa_{tp} + \beta_{tp} b \tag{11}$$

$$PE(b) = \kappa_{pe} + \beta_{pe} b \tag{12}$$

where b represents the overall block number in session 1 and 2, κ represents initial performance, and β represents the learning rate for each component. For all metrics, a positive β indicates better performance and a significant learning component.

2) Robot Control: In the third session, subjects are evaluated on how quickly they perform all three precision tasks with the robot. This may be influenced by a number of immeasurable factors such as strategy and adaptation to the physical constraints of the robot. It may also be influenced by measurable factors such as performance in the virtual tasks, time between session 2 and session 3, and, for the experimental group, the choice of $\hat{\mathbf{W}}$. With a small number of data points, it is not expected to find a valid model of these factors to predict the final completion time. Thus, correlation coefficients between these factors and the final completion time identify relationships and rank the importance of each factor.

TABLE II
LEARNING TRENDS FITTING PARAMETERS

Metric	Group	β	β [95% CI]	κ	R^2
$CT(b)$	exp	17.10	[12.40,21.70]	177.0	0.94
	cont	1.66	[1.39, 1.92]	25.3	0.98
$TP(b)$	exp	0.024	[0.019, 0.029]	0.06	0.98
	cont	0.033	[0.028, 0.038]	0.26	0.97
$PE(b)$	exp	0.031	[0.024, 0.038]	0.20	0.10
	cont	0.037	[0.032, 0.042]	0.53	0.23

*exp: experimental group; cont: control group

IV. RESULTS

Eight healthy subjects (all male, age 19-40, 1 left-, 7 right-handed, forearm circumference $10 - 12in$, forearm length $9.75-11.25in$) formed the experimental group. Five additional subjects (all male, age 20-25) served as the control group. All subjects gave informed consent to the procedures as approved by the ASU IRB (Protocol: #1201007252).

Of the eight subjects in the experimental group, two subjects displayed outlier tendencies. One subject experienced sudden confusion during the second session (block 6), which caused a loss of control. This subject struggled to regain control throughout the remaining experiment. In contrast, another participant learned the controls almost entirely in the 20 minute exploration stage and performed significantly better than any other subject, even those in the control group, throughout all sessions. The results include both subjects, most noticeably through the learning trend inconsistencies at block 6

A. Learning Trends

The average time between session 1 and 2 was 30 hours for the experimental group, and 25 hours for the control group. All but one subject found the controls easier at the start of the session 2, consistent with motor learning characteristics [63].

Completion times for both groups follow a roughly linear trend throughout sessions 1 and 2 (see Fig. 7 top). The fit for the experimental group reveals a significant learning rate despite the non-intuitive control scheme resulting in initial poor performance (see Table II first row). The control group also shows a significant learning rate, though significantly less than the experimental group, as subjects found the noiseless keyboard inputs easier to explore and quicker to learn. Consistent with previous studies [30], [33], the two groups quickly trend toward similar performance despite the initial gap.

The two groups similarly show significant learning trends in throughput (see Fig. 7 middle). The learning rates for both the experimental group and control group are not significantly different, (see Table II row 2), although they are separated by an initial performance gap relating to the ease of discovering the appropriate control inputs.

Both groups also show significant learning in path efficiency (see Fig. 7 bottom). The learning rates for both the experimental group and control group are not significantly different (see Table II row 3), although they are separated by the initial performance gap, similar to throughput. The poor fit metrics are expected due to the bias toward higher variance as the mean path efficiency increases [34].

Both groups maintained the learning trends despite the break between sessions, as shown by block 4 and 5 in Fig. 7.

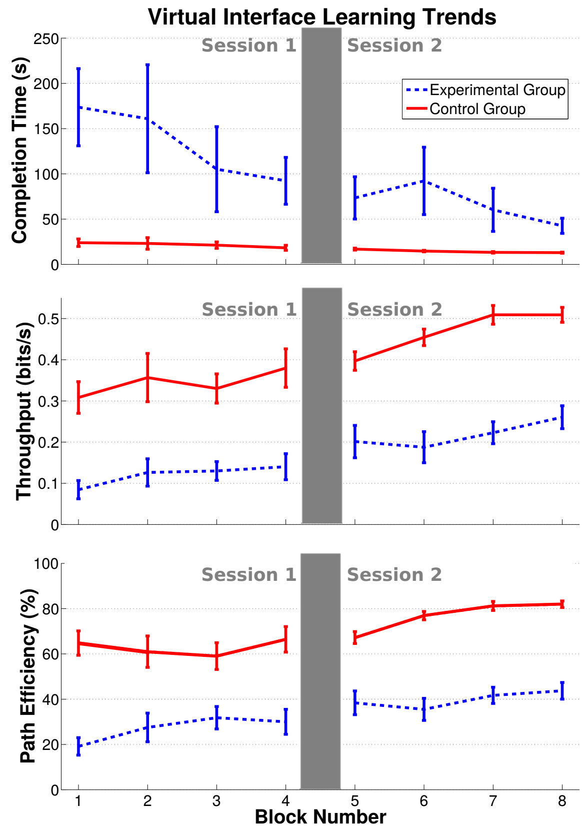

Fig. 7. Performance metrics as a function of block number for all subjects. The error-bars represent a 95% confidence interval within each block. Both groups display consistent improvement despite at least 24 hours between each session. With respect to completion times, the experimental group shows worse initial performance but a faster learning rate such that completion times are quickly converging. Both groups have similar learning rates in throughput and path efficiency, with an offset indicative of the additional exploration time needed for sEMG controls.

B. Robot Control

The average time between session 2 and 3 was 97 hours ($\sim$ 4 days) for the experimental group, and 119 hours ($\sim$ 5 days) for the control group. All but one subject found the controls consistent during the start of the third session, although all subjects in both groups perceived occasional delays in the control outputs, caused by generating outputs exceeding physical joint and velocity limits. An example grasp sequence is shown in Fig. 8. A supplementary video demonstrating the various precision tasks is available at: http://youtu.be/Qrel34jA4TQ.

On average, the control group finished all three tasks in 14.4 minutes (95% CI [10.8, 18.0]), while the experimental group finished in 30.6 minutes (95% CI [18.0, 43.1]). Although significantly higher on a student paired t-test ($p = 0.04$), the relative completion times, with the experimental group finishing twice as long as the control group, are expected considering the trends in Fig. 7. At the end of session 2, the experimental group finished tasks three times slower than the control group, but was trending toward equal performance.

The relationship between the final completion time and identified sources of influence are considered by correlation coefficients between the metrics for each subject, displayed in Table III. For both groups, the only significant correlation is with throughput ($p < 0.05$). Completion time and path

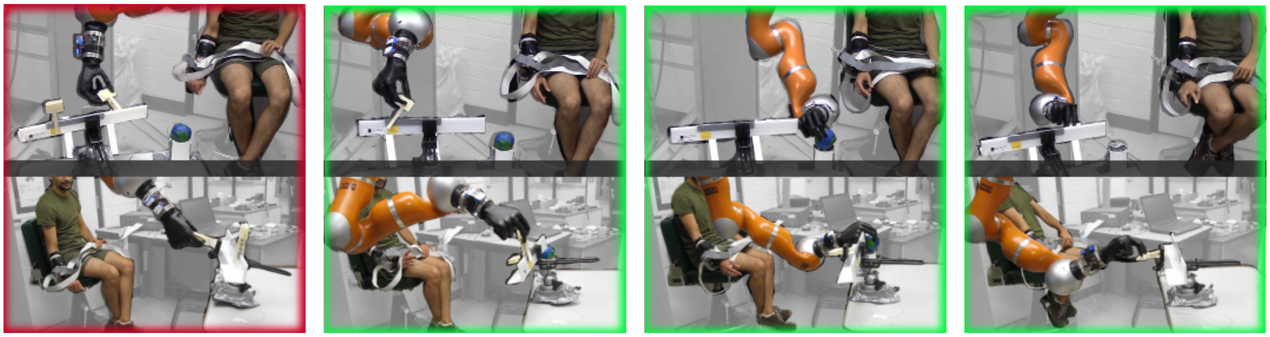

(a) (b) (c) (d)

Fig. 8. Example chronological task sequence completed by a subject, with an example of an unsuccessful grasp (a) in red, followed by three successful grasps (b, c, d) in green, demonstrating the precision required to complete the tasks.

TABLE III
INFLUENTIAL FACTORS IN ROBOT COMPLETION TIME

Factor	Experimental (R)	Control (R)
Throughput	-0.82	-0.75
Completion Time	+0.70	+0.66
Path Efficiency	-0.61	-0.61
Delay	-0.16	-0.41
$\hat{\mathbf{W}}$	-0.28	–

efficiency at the end of session 2 are moderately correlated with final completion time ($p < 0.1$). In contrast, the delay between session 2 and session 3 is- not correlated with the final completion time ($p = 0.71$), which suggests performance degradation is not a significant factor in completion times. The choice of $\hat{\mathbf{W}}$ is considered with respect to both activation component-wise and merged-component cosine similarity to the subject with significantly better control than any other subject. This produces only weak correlations ($p > 0.4$), indicating that the exact $\hat{\mathbf{W}}$ is not a significant influence. An analysis of electrode span and distance between activation components, expected to be the major factors influencing robustness, also gave weak correlations with performance ($p > 0.5$), likely due to variability across subjects. Future work will investigate these relationships more closely.

V. DISCUSSION

This work presents a novel motor learning-based control scheme capable of real-time simultaneous and proportional control of a large number of DoFs without requiring retraining between sessions. Using high density sEMG, a muscle synergy-inspired decomposition avoids the constraint on targeted electrode placement while maintaining the session-independent benefits shown in other motor learning-based control schemes. Despite not knowing either the input signals nor non-intuitive mapping, the subjects demonstrate learning trends consistent with typical motor skill learning. The same trends are seen with the control group using noiseless keyboard inputs, and are consistent with previous works which control fewer DoFs while targeting specific muscles [30]–[32], [34], [38].

The proposed method is designed to be robust to small electrode displacements by approximating independent activation signals as mixtures of Gaussians, effectively introducing a spatial low-pass filter on noisy EMG while reducing them to more stable, low-dimensional inputs. Thus, robustness of the method is a function of electrode span within and distance between each activation signal. Future work will quantify robustness with respect to these two variables and measured electrode displacement, as in [57].

Two potential outliers were revealed in this study. One subject became confused in the middle of a session, and had to restart the exploration process to re-learn the controls. Another subject performed significantly better than the control group throughout the experiment. This subject finished session 3 in six minutes and reported the controls to be both intuitive and simple to use. As the only subject with significant video gaming experience, this supports findings that video gamers learn myoelectric control tasks faster [46], perhaps due to enhanced ability to explore the potential input space.

This study focuses on solely able-bodied subjects to validate the proposed method as a practical control scheme for general myoelectric interfaces. However, the concepts of motor learning and brain plasticity may also be applicable to amputees and subjects with muscular disorders [5]. These groups may not have voluntary control over muscles necessary for conventional intuitive controls with high functionality. By generating a $\hat{\mathbf{W}}$ which maximizes the number of independent activation signals, assistive myoelectric devices might offer a sense of intuitive control without requiring kinematic mappings [45], at the expense of the initial learning curve associated with motor learning. This will be explored in future work.

The performance of each subject with the VR interfaces correlates with the ability to control precision tasks with the robot, despite subjects feeling differences in the control scheme due to physical constraints. In particular, speed and accuracy, as measured by TP, significantly reflected their capabilities in the physical interface. This implies that VR may be used to implicitly train subjects to intuitively interact with a physical robot, as in [38]. It also suggests that VR can be used as an initial screening to determine the viability of a motor learning-based control scheme (i.e. overcoming the initial learning curve) for a potential user.

In summary, the proposed control scheme provides session-independent simultaneous and proportional control of myoelectric interfaces using muscle synergy-inspired inputs. These inputs reduce the constraint on exact electrode placement over muscles, and increase the potential functionality of motor learning-based control approaches. The controls can be enhanced simply by interacting with the interface, similarly to learning a new motor skill. The results confirm significant learning trends correlating with a sense of more intuitive control, supporting this method as a viable technique for reliable long-term control of myoelectric interfaces.

References

[1] M. Ison and P. Artemiadis, "The role of muscle synergies in myoelectric control: trends and challenges for simultaneous multifunction control," *Journal of Neural Engineering*, vol. 11, no. 5, p. 051001, Oct 2014.

[2] E. Scheme and K. Englehart, "Electromyogram pattern recognition for control of powered upper-limb prostheses: state of the art and challenges for clinical use." *The Journal of Rehabilitation Research and Development*, vol. 48, no. 6, pp. 643–659, 2011.

[3] A. E. Schultz and T. A. Kuiken, "Neural interfaces for control of upper limb prostheses: the state of the art and future possibilities," *PM&R*, vol. 3, no. 1, pp. 55–67, 2011.

[4] P. K. Artemiadis and K. J. Kyriakopoulos, "A Switching Regime Model for the EMG-Based Control of a Robot Arm," *IEEE Transactions on Systems Man and Cybernetics Part B (Cybernetics)*, vol. 41, no. 1, pp. 53–63, Feb 2011.

[5] J. Vogel, J. Bayer, and P. van der Smagt, "Continuous robot control using surface electromyography of atrophic muscles," in *Intelligent Robots and Systems (IROS), IEEE/RSJ International Conference on*, 2013, pp. 845–850.

[6] A. Ajoudani, S. Godfrey, M. Catalano, G. Grioli, N. Tsagarakis, and A. Bicchi, "Teleimpedance control of a synergy-driven anthropomorphic hand," in *Intelligent Robots and Systems (IROS), 2013 IEEE/RSJ International Conference on*. IEEE, Nov 2013, pp. 1985–1991.

[7] I. Moon, M. Lee, J. Chu, and M. Mun, "Wearable EMG-based HCI for Electric-Powered Wheelchair Users with Motor Disabilities," in *Robotics and Automation (ICRA). Proceedings of the 2005 IEEE International Conference on*. IEEE, 2005, pp. 2649–2654.

[8] M. S. Erkilinc and F. Sahin, "Camera control with EMG signals using Principal Component Analysis and support vector machines," in *Systems Conference (SysCon), IEEE International*, Apr 2011, pp. 417–421.

[9] L. H. Smith, T. A. Kuiken, and L. J. Hargrove, "Real-time simultaneous and proportional myoelectric control using intramuscular emg," *Journal of neural engineering*, vol. 11, no. 6, p. 066013, 2014.

[10] M. Atzori, A. Gijsberts, C. Castellini, B. Caputo, A.-G. M. Hager, S. Elsig, G. Giatsidis, F. Bassetto, and H. Müller, "Electromyography data for non-invasive naturally-controlled robotic hand prostheses," *Scientific Data*, vol. 1, 2014.

[11] J. Liu, X. Sheng, D. Zhang, J. He, and X. Zhu, "Reduced daily recalibration of myoelectric prosthesis classifiers based on domain adaptation," *Biomedical and Health Informatics, IEEE Journal of*, vol. PP, no. 99, pp. 1–1, December 2014.

[12] X. Zhang and H. Huang, "A real-time, practical sensor fault-tolerant module for robust emg pattern recognition," *Journal of NeuroEngineering and Rehabilitation*, vol. 12, no. 1, p. 18, 2015.

[13] A. D. Roche, H. Rehbaum, D. Farina, and O. C. Aszmann, "Prosthetic myoelectric control strategies: A clinical perspective," *Current Surgery Reports*, vol. 2, no. 3, pp. 1–11, Mar 2014.

[14] C. Cipriani, F. Zaccone, S. Micera, and M. Carrozza, "On the Shared Control of an EMG-Controlled Prosthetic Hand: Analysis of User-Prosthesis Interaction," *IEEE Transactions on Robotics*, vol. 24, no. 1, pp. 170–184, Feb 2008.

[15] A. J. Young, L. H. Smith, E. J. Rouse, and L. J. Hargrove, "A comparison of the real-time controllability of pattern recognition to conventional myoelectric control for discrete and simultaneous movements," *Journal of neuroengineering and rehabilitation*, vol. 11, no. 1, p. 5, 2014.

[16] M. Ortiz-Catalan, B. Hakansson, and R. Branemark, "Real-time and simultaneous control of artificial limbs based on pattern recognition algorithms," *Neural Systems and Rehabilitation Engineering, IEEE Transactions on*, vol. 22, no. 4, pp. 756–764, July 2014.

[17] J. Hahne, F. BieBmann, N. Jiang, H. Rehbaum, D. Farina, F. Meinecke, K.-R. Muller, and L. Parra, "Linear and nonlinear regression techniques for simultaneous and proportional myoelectric control," *Neural Systems and Rehabilitation Engineering, IEEE Transactions on*, vol. 22, no. 2, pp. 269–279, March 2014.

[18] E. Scheme, A. Fougner, Ø. Stavdahl, A. Chan, and K. Englehart, "Examining the adverse effects of limb position on pattern recognition based myoelectric control," in *Engineering in Medicine and Biology Society (EMBC), Annual International Conference of the IEEE*, 2010, pp. 6337–6340.

[19] P. K. Artemiadis and K. J. Kyriakopoulos, "An EMG-Based Robot Control Scheme Robust to Time-Varying EMG Signal Features," *IEEE Transactions on Information Technology in Biomedicine*, vol. 14, no. 3, pp. 582–588, May 2010.

[20] L. Hargrove, K. Englehart, and B. Hudgins, "The effect of electrode displacements on pattern recognition based myoelectric control," in *Engineering in Medicine and Biology Society. 28th Annual International Conference of the IEEE*, 2006, pp. 2203–2206.

[21] K. Nazarpour, A. Sharafat, and S. Firoozabadi, "Negentropy analysis of surface electromyogram signal," in *Statistical Signal Processing, 2005 IEEE/SP 13th Workshop on*, july 2005, pp. 974–977.

[22] A. Gijsberts, R. Bohra, D. Sierra González, A. Werner, M. Nowak, B. Caputo, M. A. Roa, and C. Castellini, "Stable myoelectric control of a hand prosthesis using non-linear incremental learning," *Frontiers in Neurorobotics*, vol. 8, no. 8, pp. 1–15, 2014.

[23] X. Chen, D. Zhang, and X. Zhu, "Application of a self-enhancing classification method to electromyography pattern recognition for multifunctional prosthesis control," *Journal of NeuroEngineering and Rehabilitation*, vol. 10, no. 1, p. 44, 2013.

[24] J. W. Sensinger, B. A. Lock, and T. A. Kuiken, "Adaptive pattern recognition of myoelectric signals: exploration of conceptual framework and practical algorithms," *Neural Systems and Rehabilitation Engineering, IEEE Transactions on*, vol. 17, no. 3, pp. 270–278, 2009.

[25] P. M. Pilarski, M. R. Dawson, T. Degris, F. Fahimi, J. P. Carey, and R. S. Sutton, "Online human training of a myoelectric prosthesis controller via actor-critic reinforcement learning," in *Rehabilitation Robotics (ICORR), 2011 IEEE International Conference on*. IEEE, 2011, pp. 1–7.

[26] A. E. Gibson, M. R. Ison, and P. Artemiadis, "User-Independent Hand Motion Classification with Electromyography," in *2013 Dynamic Systems and Control Conference (DSCC)*, vol. 2. ASME, October 2013, pp. V002T26A002; 1–6.

[27] M. R. Ison and P. Artemiadis, "Beyond User-Specificity for EMG Decoding Using Multiresolution Muscle Synergy Analysis," in *2013 Dynamic Systems and Control Conference (DSCC)*, vol. 1. ASME, October 2013, pp. V001T08A006: 1–6.

[28] R. Khushaba, "Correlation analysis of electromyogram signals for multiuser myoelectric interfaces," *Neural Systems and Rehabilitation Engineering, IEEE Transactions on*, vol. 22, no. 4, pp. 745–755, July 2014.

[29] T. Matsubara and J. Morimoto, "Bilinear modeling of emg signals to extract user-independent features for multiuser myoelectric interface," *Biomedical Engineering, IEEE Transactions on*, vol. 60, no. 8, pp. 2205–2213, Aug 2013.

[30] S. M. Radhakrishnan, S. N. Baker, and A. Jackson, "Learning a novel myoelectric-controlled interface task," *Journal of Neurophysiology*, vol. 100, no. 4, pp. 2397–2408, Aug 2008.

[31] M. Ison, C. W. Antuvan, and P. Artemiadis, "Learning efficient control of robots using myoelectric interfaces," in *Robotics and Automation (ICRA), 2014 IEEE International Conference on*, May 2014, pp. 2880–2885.

[32] T. Pistohl, C. Cipriani, A. Jackson, and K. Nazarpour, "Abstract and Proportional Myoelectric Control for Multi-Fingered Hand Prostheses," *Annals of Biomedical Engineering*, vol. 41, no. 12, pp. 2687–2698, Dec 2013.

[33] C. W. Antuvan, M. Ison, and P. Artemiadis, "Embedded human control of robots using myoelectric interfaces," *IEEE Transactions on Neural Systems and Rehabilitation Engineering*, vol. 22, no. 4, pp. 820–827, Jul 2014.

[34] M. Ison and P. Artemiadis, "Proportional Myoelectric Control of Robots: Muscle Synergy Development drives Performance Enhancement, Retainment, and Generalization," *Robotics, IEEE Transactions on*, 2015 (in press).

[35] K. Nazarpour, A. Barnard, and A. Jackson, "Flexible Cortical Control of Task-Specific Muscle Synergies," *Journal of Neuroscience*, vol. 32, no. 36, pp. 12 349–12 360, Sep 2012.

[36] A. de Rugy, G. E. Loeb, and T. J. Carroll, "Muscle Coordination Is Habitual Rather than Optimal," *Journal of Neuroscience*, vol. 32, no. 21, pp. 7384–7391, May 2012.

[37] A. de Rugy, G. E. Loeb, and T. J. Carroll, "Are muscle synergies useful for neural control ?" *Frontiers in Computational Neuroscience*, vol. 7, no. 19, pp. 1–13, 2013.

[38] M. Ison and P. Artemiadis, "Enhancing Practical Multifunctional Myoelectric Applications through Implicit Motor Control Training Systems," in *Engineering in Medicine and Biology Society (EMBC), International Conference of the IEEE*, 2014, pp. 3525–3528.

[39] N. Jiang, K. B. Englehart, and P. A. Parker, "Extracting simultaneous and proportional neural control information for multiple-DOF prostheses from the surface electromyographic signal," *IEEE Transactions on Biomedical Engineering*, vol. 56, no. 4, pp. 1070–1080, Apr 2009.

[40] P. Artemiadis and K. Kyriakopoulos, "EMG-Based Control of a Robot Arm Using Low-Dimensional Embeddings," *Robotics, IEEE Transactions on*, vol. 26, no. 2, pp. 393–398, april 2010.

[41] J. Vogel, C. Castellini, and P. van der Smagt, "EMG-based teleoperation and manipulation with the DLR LWR-III," in *Intelligent Robots and Systems (IROS), IEEE/RSJ International Conference on*, sept. 2011, pp. 672–678.

[42] P. M. Fitts and M. I. Posner, *Human performance.* Brooks/Cole, 1967.

[43] J. M. Carmena, "Advances in neuroprosthetic learning and control," *PLoS biology*, vol. 11, no. 5, p. e1001561, 2013.

[44] J. d. R. Millán, "Brain-computer interfaces," in *Introduction to Neural Engineering for Motor Rehabilitation*, D. Farina, W. Jensen, and M. Akay, Eds. Hoboken, NJ: John Wiley and Sons, 2013, vol. 40, pp. 237–253.

[45] N. Jiang, I. Vujaklija, H. Rehbaum, B. Graimann, and D. Farina, "Is accurate mapping of emg signals on kinematics needed for precise online myoelectric control?" *IEEE Transactions on Neural Systems and Rehabilitation Engineering*, vol. 22, no. 3, pp. 549–558, May 2014.

[46] R. Clingman and P. Pidcoe, "A novel myoelectric training device for upper limb prostheses," *Neural Systems and Rehabilitation Engineering, IEEE Transactions on*, vol. 22, no. 4, pp. 879–885, July 2014.

[47] I. Ahmad, F. Ansari, and U. Dey, "A review of emg recording technique," *International Journal of Engineering Science and Technology*, vol. 4, no. 2, pp. 530–539, 2012.

[48] D. Farina, N. Jiang, H. Rehbaum, A. Holobar, B. Graimann, H. Dietl, and O. C. Aszmann, "The extraction of neural information from the surface emg for the control of upper-limb prostheses: Emerging avenues and challenges," *IEEE Transactions on Neural Systems and Rehabilitation Engineering*, vol. 22, no. 4, pp. 797–809, Jul 2014.

[49] C. Cipriani, J. Segil, J. Birdwell, and R. Weir, "Dexterous control of a prosthetic hand using fine-wire intramuscular electrodes in targeted extrinsic muscles," *Neural Systems and Rehabilitation Engineering, IEEE Transactions on*, vol. 22, no. 4, pp. 828–836, July 2014.

[50] E. J. Scheme and K. B. Englehart, "Validation of a selective ensemble-based classification scheme for myoelectric control using a three-dimensional fitts' law test," *Neural Systems and Rehabilitation Engineering, IEEE Transactions on*, vol. 21, no. 4, pp. 616–623, 2013.

[51] N. Jiang, J. L. Vest-Nielsen, S. Muceli, D. Farina *et al.*, "Emg-based simultaneous and proportional estimation of wrist/hand kinematics in uni-lateral trans-radial amputees," *Journal of neuroengineering and rehabilitation*, vol. 9, no. 1, p. 42, 2012.

[52] J. M. Hahne, H. Rehbaum, F. Biessmann, F. C. Meinecke, K. Muller, N. Jiang, D. Farina, and L. C. Parra, "Simultaneous and proportional control of 2d wrist movements with myoelectric signals," in *Machine Learning for Signal Processing (MLSP), 2012 IEEE International Workshop on*, Sept 2012, pp. 1–6.

[53] S. Muceli and D. Farina, "Simultaneous and proportional estimation of hand kinematics from emg during mirrored movements at multiple degrees-of-freedom," *Neural Systems and Rehabilitation Engineering, IEEE Transactions on*, vol. 20, no. 3, pp. 371–378, 2012.

[54] D. Tkach, A. Young, L. Smith, E. Rouse, and L. Hargrove, "Real-time and offline performance of pattern recognition myoelectric control using a generic electrode grid with targeted muscle reinnervation patients," *Neural Systems and Rehabilitation Engineering, IEEE Transactions on*, vol. 22, no. 4, pp. 727–734, July 2014.

[55] C. Choi and J. Kim, "Synergy matrices to estimate fluid wrist movements by surface electromyography," *Medical engineering & physics*, vol. 33, no. 8, pp. 916–923, 2011.

[56] N. Jiang, H. Rehbaum, I. Vujaklija, B. Graimann, and D. Farina, "Intuitive, online, simultaneous and proportional myoelectric control over two degrees-of-freedom in upper limb amputees," *IEEE Transactions on Neural Systems and Rehabilitation Engineering*, vol. 22, no. 3, pp. 501–510, May 2014.

[57] S. Muceli, N. Jiang, and D. Farina, "Extracting signals robust to electrode number and shift for online simultaneous and proportional myoelectric control by factorization algorithms," *Neural Systems and Rehabilitation Engineering, IEEE Transactions on*, vol. 22, no. 3, pp. 623–633, May 2014.

[58] [Online]. Available: http://www.opengl.org

[59] A. S. Luchins, "Mechanization in problem solving: The effect of einstellung." *Psychological monographs*, vol. 54, no. 6, p. i, 1942.

[60] A. Simon, L. Hargrove, B. Lock, and T. Kuiken, "A Decision-Based Velocity Ramp for Minimizing the Effect of Misclassifications During Real-Time Pattern Recognition Control," *IEEE Transactions on Biomedical Engineering*, vol. 58, no. 8, pp. 2360–2368, Aug 2011.

[61] S. Wurth and L. Hargrove, "Real-time comparison of conventional direct control and pattern recognition myoelectric control in a two-dimensional fitts' law style test," in *Engineering in Medicine and Biology Society (EMBC), 2013 35th Annual International Conference of the IEEE*, 2013, pp. 3630–3633.

[62] R. W. Soukoreff and I. S. MacKenzie, "Towards a standard for pointing device evaluation, perspectives on 27 years of fitts' law research in hci," *Int. J. Hum.-Comput. Stud.*, vol. 61, no. 6, pp. 751–789, Dec. 2004.

[63] M. P. Walker, T. Brakefield, A. Morgan, J. A. Hobson, and R. Stickgold, "Practice with sleep makes perfect: sleep-dependent motor skill learning," *Neuron*, vol. 35, no. 1, pp. 205–211, 2002.